Proc. R. Soc. Lond. A **399**, 93–109 (1985)
Printed in Great Britain

On the microwave reflectivity of small-scale breaking water waves

By M. L. Banner[1] and E. H. Fooks[2]

[1] *School of Mathematics, University of New South Wales, P.O. Box* 1, *Kensington, New South Wales, Australia* 2033
[1] *Ocean Sciences Division, Royal Australian Navy Research Laboratory, P.O. Box* 706, *Darlinghurst, New South Wales, Australia* 2010
[2] *School of Electrical Engineering and Computer Science, University of New South Wales, P.O. Box* 1, *Kensington, New South Wales, Australia* 2033

(*Communicated by O. M. Phillips, F.R.S. – Received* 10 *April* 1984)

The aim of this paper is to elucidate the microwave reflectivity properties of small-scale breaking water waves, which are a widespread feature of the wind-driven air–sea interface. By using a laboratory wave flume in which a small-scale breaking wave was held stationary against an opposing current, a detailed investigation of the microwave reflectivity at X-band revealed significantly enhanced levels of local backscattered power from the crest regions of small-scale breaking waves. A surprising level of organization is discovered in the hydrodynamic disturbances generated in such breaking zones. Their wavenumber–frequency spectral properties are reported in detail, from which it is concluded that the microwave reflectivity is consistent with Bragg scattering from these disturbances. The application of these findings to active microwave remote sensing of the oceans is discussed.

1. Introduction

Microwave backscatter from the sea surface forms the basis of techniques developed recently for remotely sensing dominant ocean waves and windstress from satellites. Certain instruments that use these techniques (synthetic aperture radar for imaging ocean waves, scatterometer for sensing the wind stress) have been deployed on the N.A.S.A. oceanographic satellite Seasat, which was operational for 100 days in 1978. Much of the Seasat data has been analysed with approximate operational algorithms that relate the microwave backscattered cross section to the oceanographic variable of interest; either the waveheight (wavenumber) spectrum or the windstress vector. When normalized, these data compare favourably with ground truth data from approximately collocated conventional measurements obtained from surface experiments in progress during Seasat overpasses. To be able to relate the backscattered cross section to the waveheight or windstress on an absolute basis, a more detailed understanding of the mechanisms involved in microwave backscattering from the ocean surface is required. This is evident from the recent field experiment by Wright *et al.* (1980). They reported

modulation transfer functions of microwave backscattered power at 9.375 and 1.5 GHz as a function of ocean wave frequency and of windspeed. The observed magnitude and phase of the modulation transfer function were inadequately predicted by the relaxation model of Keller *et al.* (1975) for the orbital straining of the resonant Bragg waves. Having taken into account wave-related effects such as tilting and range variation, Wright *et al.* (1980) concluded that the modulation of short gravity–capillary waves, including the Bragg waves, by ocean waves with periods of the order of 10 s is due to a source substantially stronger than the straining of the short waves by the horizontal component of orbital speed of the long waves. It should be noted that this conclusion is based on the microwave modulation levels and not on direct short gravity–capillary wave measurements. More recently, Monaldo *et al.* (1982) presented optically determined modulation transfer functions for short wavelengths of 30, 115 and 300 mm under the action of a wind of 5 m s^{-1} and underlying long waves with a slope of approximately 0.06, which resulted in modulations of magnitude 9 $(\text{slope})^{-1}$ and phase 90° leading the long wave crest for each of the short wavelengths studied. With Wright *et al.* (1980) reporting microwave modulating functions with magnitudes from 5 $(\text{slope})^{-1}$ to 30 $(\text{slope})^{-1}$ and phases from 5° to 80° for 9.375 GHz and about one-half these values in both magnitude and phase for 1.5 GHz, it is apparent that basic questions still remain on the relation between microwave backscatter modulation levels and the modulation of short-wave spectral components by longer ocean waves and windstress.

Implicit in the conclusions of Wright *et al.* (1980) is the dominance of the Bragg resonant backscattering mechanism, established firmly by the U.S. Naval Research Laboratory (N.R.L) group as the primary backscattering mechanism in their series of laboratory wind-wave investigations using focused parabolic microwave antennae. The N.R.L. report of Wright *et al.* (1972) on wind-wave studies, also published as Duncan *et al.* (1974), provides a detailed account of microwave Doppler spectra from Bragg scattering under a range of microwave viewing conditions in their wind-wave tank. Under Bragg resonance conditions, the parabolic microwave antenna acts as a selective (vector) wavenumber probe, responding ideally only to the water-wave spectral components that satisfy

$$\boldsymbol{k}_{\mathrm{w}} = (2k_0 \cos\theta, 0), \tag{1}$$

where k_0 is the microwave wavenumber magnitude and the antenna is looking in the upwind–downwind direction at a depression angle of θ. Owing to the finite extent of the zone illuminated by the antenna, there is a small range of water-wave spectral components near the $\boldsymbol{k}_{\mathrm{w}}$, which are involved in the backscattering. Accordingly, from Plant & Wright (1977), the backscattered power spectral density $P(k_0, \theta, \omega)$ is related to the surface displacement spectrum $F(\boldsymbol{k}, \omega)$ by the convolution of the latter with the antenna illumination function $V(\boldsymbol{k})$:

$$P(k_0, \theta, \omega) = g(\theta) \int F(\boldsymbol{k}, \omega)\, V(\boldsymbol{k}_{\mathrm{w}} - \boldsymbol{k})\, \mathrm{d}\boldsymbol{k}, \tag{2}$$

where $g(\theta)$ depends also on the polarization and dielectric constant.

Doppler spectra generated from the microwave return determine the frequencies

and phase speeds of the Bragg scatterers. For their wave tank conditions, Wright *et al.* (1972) report that for small to moderate depression angles the dominant scatterers were found generally to travel at a phase speed close to the free water-wave speed with the difference attributed to wind drift effects. For larger depression angles and higher windspeeds, however, dominant scatterers bound to the dominant water-wave speed were mostly observed. Although their results were obtained mainly for vertical polarization of the transmitted and received beam, their report points out the existence and dominance of strong microwave scatterers other than 'free' Bragg waves under a range of conditions. In their report (pp. 9–12), the fundamental question of oceanic polarization ratio σ_{vv}/σ_{hh} is addressed. Here σ_{vv} and σ_{hh} are the backscattering cross sections for vertical transmit–vertical receive and horizontal transmit–horizontal receive polarizations respectively. It is pointed out that composite surface theory using first-order Bragg scattering yields a polarization ratio of 10 dB or greater, whereas polarization ratios near unity tend to be found for oceanic observations. They infer that the trend towards unity polarization ratio at high winds is largely due to scatterers moving at or near the crest speed of the dominant wind-wave in the tank and, in their concluding remarks, state 'At high winds, the bound waves are, perhaps, not waves in the visual sense at all, but rather the broken water ahead of the crests of the dominant waves.'

Other investigators have reported on microwave measurements in wave tank studies. Lee (1977) reported on microwave Doppler spectra from short wind waves at low windspeed ($u_* \approx 0.15$ m s^{-1}) at a fetch of 7.5 m by using a horn antenna with an auxiliary aperture near the water surface to localize the illuminated area. The Doppler spectra reported in figure 3 of his paper show evidence of free Bragg waves with a contribution appearing at the frequency of the dominant 6 Hz water wave, suggesting the passage of groups of Bragg waves at this frequency. A more recent study by Kwoh & Lake (1983) has reported further results aimed at a better understanding of the local microwave reflectivity of water waves. Using a conical horn with a matched dielectric lens, they examined self-modulating paddle-generated waves (no wind forcing) characterized by intermittent, gentle breaking, i.e. breaking without air entrainment. Various factors involved in the backscattering process were identified:

(i) significant backscattering occurred in discrete bursts, strongly correlated with the gentle breaking events;

(ii) the high curvature at the crest just before breaking, the attendant capillary waves ahead of the breaking zone and the turbulent wake were all contributors.

Much of their investigation and analysis was concerned with questioning the applicability of the Bragg scattering mechanism and studying other possible mechanisms that might model the physics more realistically. Among these, 'specular' reflections from the waveform characteristics described in (ii) are claimed to be important. The reader is referred to their report for further details.

One immediate conclusion from these laboratory studies is that, for a range of conditions, small-scale breaking waves can make a significant contribution to the microwave backscattered cross section.

The focus of the present contribution is on elucidating the microwave reflectivity

properties of small-scale breaking waves: it reports on a detailed investigation of the hydrodynamic surface disturbances originating in the breaking zones ahead of small-scale breaking gravity waves. In contrast to the notion of disorder intuitively associated with breaking zones, it is shown that breaking zone disturbances possess a surprising degree of organization. The dispersion characteristics of these disturbances have been determined experimentally for typical short breaking wavelengths by probing stationary breaking waves in a laboratory wind-wave flume. Complementary X-band microwave backscatter data were obtained for a range of incidence angles for both horizontal and vertical polarization. The findings are related to comparable propagating small-scale breaking wave measurements.

This study reveals significant levels of local backscattered power from small-scale breaking waves consistent with Bragg scattering from the organized hydrodynamic surface disturbances generated in the breaking zones. It also contributes new physical insight into the elusive question of the constitution of the high wavenumber region of the surface height spectrum. The paper concludes with a discussion of these findings in the context of active microwave remote sensing of ocean waves and windstress.

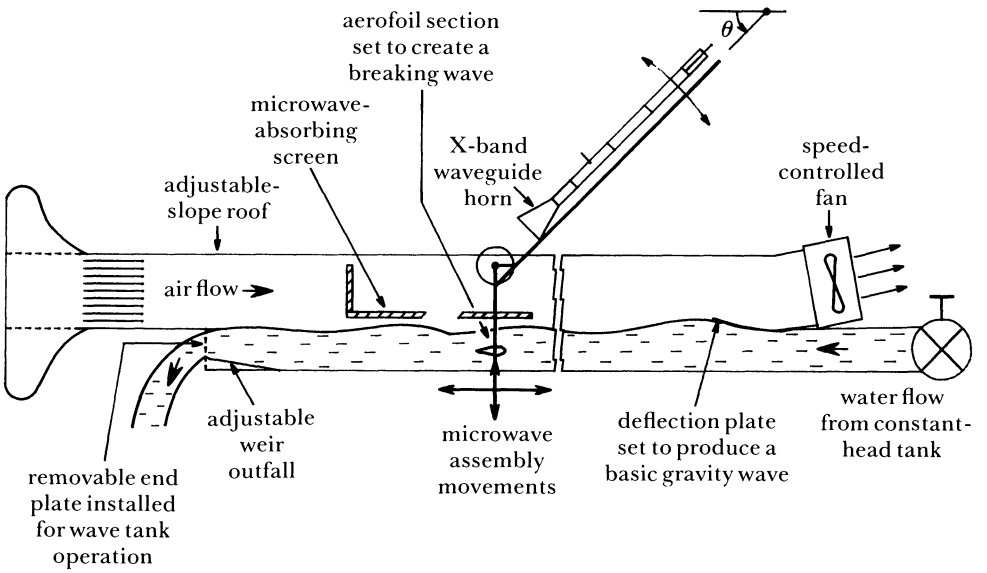

FIGURE 1. Experimental wave flume configuration: working length, 7.3 m; air channel depth, 0.36 m; water channel depth, 0.22 m; channel width, 0.225 m. The measurement site was halfway along the channel.

2. EXPERIMENTAL CONFIGURATION

Figure 1 shows the wind-wave flume configuration used in this investigation. The water flow rate and mean depth in the flume could be adjusted independently to provide a steady current up to 1 m s^{-1} at a mean depth of 0.22 m. A curved inclined plate at the entry to the working section created a train of stationary gravity waves standing against the flowing current. Using an adjustable aerofoil obstacle of

length 96 mm and chord thickness 21 mm, a steady stationary breaking wave could be induced at the measurement site, about half-wave along the flume. Careful adjustment of the depth and angle of inclination of the obstacle allowed fine-tuning of the degree of breaking, ranging from incipient to very strong: this latter condition, not studied here, had the appearance of a local hydraulic jump. The properties of the hydrodynamic disturbances under gentle breaking were investigated in this study with the obstacle inclined just beyond the point for incipient breaking of the wave immediately downstream. Two wavelengths, 0.20 and 0.33 m, were chosen as representative of small-scale breaking waves. At these scales little, if any, air entrainment or spray was present. As the obstacle was many skin depths below the water surface at 9.23 GHz, it did not have any direct influence on microwave reflection measurements. Photographs of typical breaking waves investigated are shown in figure 2.

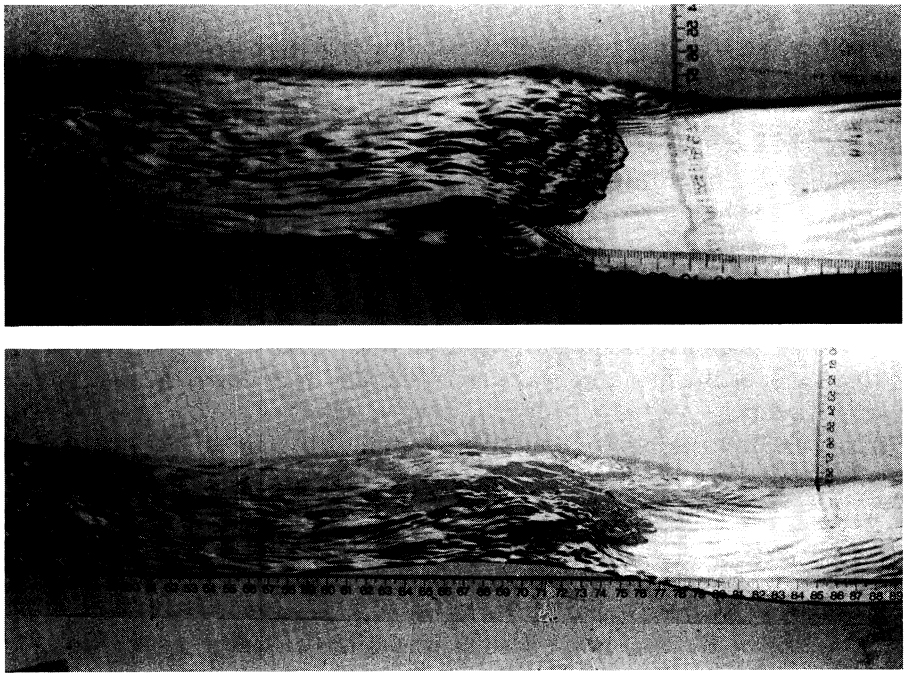

FIGURE 2. Typical stationary breaking waves with 0.20 m wavelength (top) and 0.33 m wavelength (bottom).

Exploratory microwave backscattering measurements using an X-band system revealed a strong periodicity in the return power time series when illuminating the breaking wave. This motivated the detailed probing of the breaking zone with two similar capacitance wire probes with a wire diameter of about 0.1 mm. These probes, which had linear static calibrations over their working range, were used in conjunction with a Hewlett Packard Model 3582A Spectrum Analyser interfaced to a computer to obtain longitudinal wavenumber–frequency spectra of the breaking zone disturbances. It should be noted that the breaking zones investigated

here were stationary in time, but inhomogeneous in space. Consequently, wavenumber spectra depend on the axial location in the breaking zone. For the microwave antenna looking upwind, a preliminary study indicated the region just ahead of the wave crest as the approximate site of the dominant microwave backscatter. Thus a point just ahead of the breaking wave crest was chosen as a suitable origin for representative wavenumber determinations. Longitudinal wavenumber–frequency spectra were determined as follows: probe A was held fixed at the origin while probe B was traversed longitudinally by using a traversing facility that allowed precise incremental positioning both upstream and downstream with respect to probe A. The traverses spanned $-32\,\Delta x$ to $+31\,\Delta x$ with Δx chosen to be 2 mm for the 0.20 m wavelength and 3 mm for the 0.33 m wavelength to minimize spatial aliasing. At each probe separation, ensemble averages of at least 128 individual frequency spectra were determined for the surface height of probe A and of probe B, the coherence of these two signals and their relative phase. A frequency range of 0 to 50 Hz was used on the spectrum analyser, giving a resolution of 0.4 Hz. A Hanning time window was used, giving a bandwidth of 0.6 Hz. The ensemble-averaged spectra were recorded by the computer over the frequency range of interest for subsequent off-line processing to yield frequency-separation cross-spectra. A spatial Hanning window was applied and two-sided wavenumber spectra at given frequencies were computed.

To aid further the interpretation of the breaking zone disturbance characteristics, auxiliary measurements were made as follows:

(i) longitudinal coherence frequency spectra for the fixed probe in the breaking zone and the moving probe ranging rearward over the breaking wave profile;

(ii) lateral coherence frequency spectra, with fixed probe sites in the active breaking zone, at the breaking wave crest and half way down the rear face of the breaking wave;

(iii) the mean breaking wave profile determined by one of the wave gauges.

Complementary microwave measurements were made by using the X-band (9.23 GHz) transmitter–receiver system shown in figure 1. The microwave transmitter–receiver, which used a single horn antenna for both functions, was mounted to give adjustment of the viewing position along the flume and the upwind–downwind 'look angle', pivoting about the mean water level. To localize the area sensed by the microwave system, an adjustable length aperture made from microwave-absorbing sheet was mounted on a longitudinal traverse and held about 30 mm above the mean water level. A continuous wave Gunn diode source, driven from a stabilized power supply, was maintained at a constant monitored power level and fed through a circulator to the antenna system. With the microwave system set at the desired location and with the aperture in the microwave-absorbing material closed, a slide screw tuner was adjusted to null the crystal detector on the third arm of the circulator. This cancelled out all the reflections at the operating frequency, including those from the horn and the flume as well as any microwave leakage from the source directly through the circulator. The aperture length was adjusted at each viewing angle to maintain a constant aperture of $0.10\ \text{m} \times 0.10\ \text{m}$ normal to the viewing direction. Double-sided absorbing material was used to minimize reflections and any microwave guiding between the water surface and

the rear side of the absorbing sheet. The return signal from the aperture or water surface was coupled through the circulator directly to a crystal detector which, being a square-law device, produced a signal that was proportional to the received microwave reflected power. The signal was passed through a d.c. coupled amplifier so that the output tracked the baseband variations of the received microwave reflected power.

The horn–aperture configuration does not reproduce plane wavefronts at short range, even though in the far field, particularly well. For the geometry used in this study, the phase deviation from plane fronts was estimated to be $\pm 10°$ across the aperture, at a range of 0.6 m. The lack of a capability of producing plane wavefronts placed a limitation on the amount of useful microwave data that could be collected in this study. However, the results attainable are adequate to support the major conclusions of this paper.

Microwave backscattered power spectra were recorded for each breaking wavelength with the field of view centred just ahead of the breaking wave crest and for a range of depression angles. This data was taken only for the no-wind case, because it was difficult to maintain the aperture in place near the water surface under strong wind action. As a control, a steep, almost breaking, wave was viewed in the same way. The spectral signatures of these measurements are compared with each other and with the breaking zone hydrodynamic disturbance spectra in §3.2.

Additional microwave measurements were made for the 0.20 m breaking and non-breaking waves by using a fixed depression angle of 50°, looking upwind for vertical polarization of the microwave transmitter–receiver. For an aperture width of 0.10 m, the microwave system and aperture combination were traversed along the wave profile and the spatial distribution of the mean backscattered power was recorded. By integrating under this distribution, the mean backscattered power was obtained for both breaking and steep unbroken waves of similar proportions.

To relate the stationary wave findings to the usually encountered propagating wave case, the wave flume was converted to a wave tank by blocking off the exit plane of the water channel. A wave generator was installed and driven to produce a steep 3 Hz propagating wavetrain. A 7.5 m s^{-1} wind, drawn over this wavetrain, produced an almost continuously breaking wave situation with wavelengths close to 0.20 m. A modified aperture with the vertical section removed was held in place (with difficulty) and time series of the microwave backscattered power were recorded and were also fed to a Thermosystems Model 1076 averaging digital voltmeter to obtain temporally averaged mean backscattered microwave power levels for comparison with the microwave configuration as described in the previous paragraph. In addition, time series of the microwave backscattered power return and surface elevation were recorded simultaneously on an ultraviolet oscillograph. To avoid any interference of the wave gauge with the microwave beam, the surface elevation was sensed at the same axial position as the microwave line of sight with the mean water level by a linear position photodiode with a 1 mm wide vertical aperture mounted on the glass sidewall. Illuminating the meniscus from below provided the detected signal. This technique for monitoring the elevation was checked against a conventional wave gauge and found to be

extremely reliable. It was used for referencing the microwave signal to the phase of the 3Hz breaking waves. Frequency spectra of the microwave backscattered power and of the laterally collocated surface elevation were also monitored on the spectrum analyser. Though detected at a sidewall, the optically determined waveheight signal reveals higher frequency components, predominantly on the crests. An intercomparison of the propagating and stationary breaking wave results is given in §3.2.

3. Results

3.1. *Hydrodynamic breaking zone disturbances*

For the two breaking wavelengths investigated, 0.20 and 0.33 m, frequency spectra of the free surface oscillations at different axial locations along the breaking wave profile are shown in figures 3 and 4.

It is seen immediately that, for each breaking wavelength at its given quasi-steady state of breaking, the free surface disturbance frequency spectrum possesses a

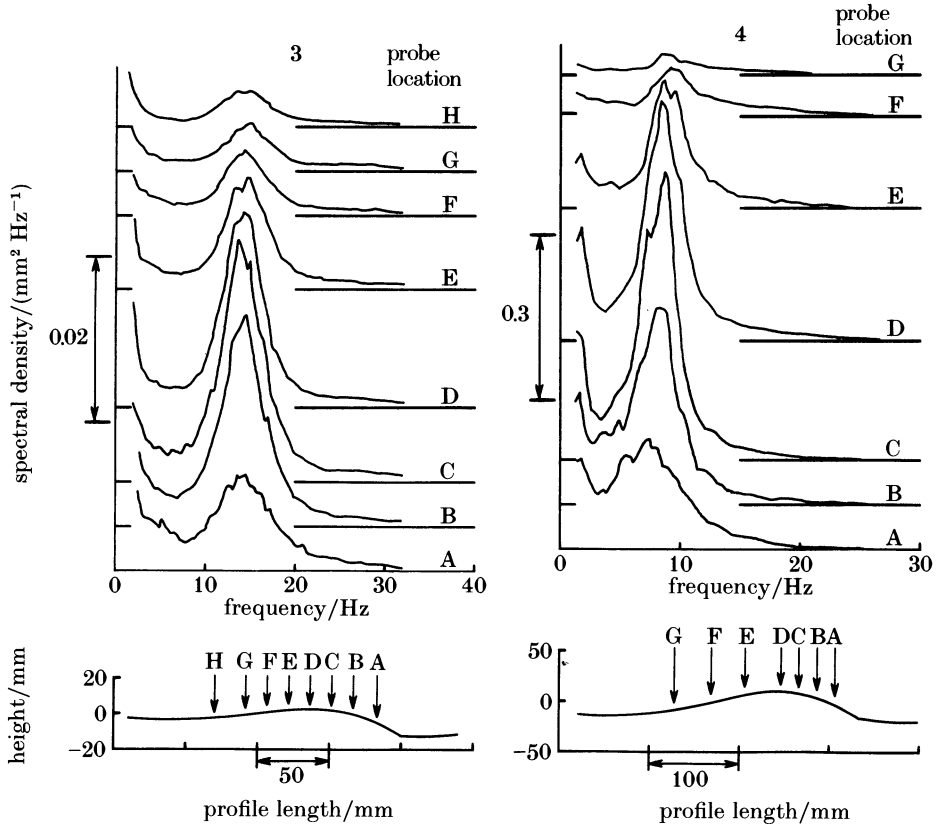

Figure 3. Variation of the surface disturbance frequency spectrum along the 0.20 m breaking wave profile.

Figure 4. Variation of the surface disturbance frequency spectrum along the 0.33 m breaking wave profile.

remarkable peakedness. From a somewhat broadened band of disturbance frequencies near the toe of the breaking wave, the spectrum grows rapidly to a sharply tuned peak, which decays in amplitude but remains stable in frequency with rearward axial distance from the crest region. The peak frequency itself was found to vary with the degree of breaking for a given breaking wavelength. For the 0.20 m breaking wave, peak frequencies in the range 12–16 Hz were observed, depending on the strength of the breaking imposed by the obstacle orientation. It should be noted that, with the submerged obstacle responsible for the excess energy causing breaking of the wave, this configuration is unlikely to simulate the case of purely wind-driven breaking in one key respect: the latter, according to the observations of Okuda *et al.* (1977) is characterized by a highly sheared, wind-driven surface layer feeding into the breaking zone. The consequences of this difference are considered in detail in §4.

Consider the dispersion characteristics of the frequency spectra, which, apart from their intrinsic physical interest, are central to the interpretation of the complementary microwave data. Figures 5 and 6 show the two-sided longitudinal wavenumber spectra for frequency components distributed around the peak for the 0.20 and 0.33 m breaking waves respectively. These show the distribution of disturbance energy with respect to the disturbance wavenumber as a function of the disturbance frequency in the vicinity of the breaking wave crest. The noise floor estimated from the disturbance spectrum in the unbroken water ahead of the breaking zone was found to be less than 2×10^{-3} mm^3 Hz^{-1} when based on a white

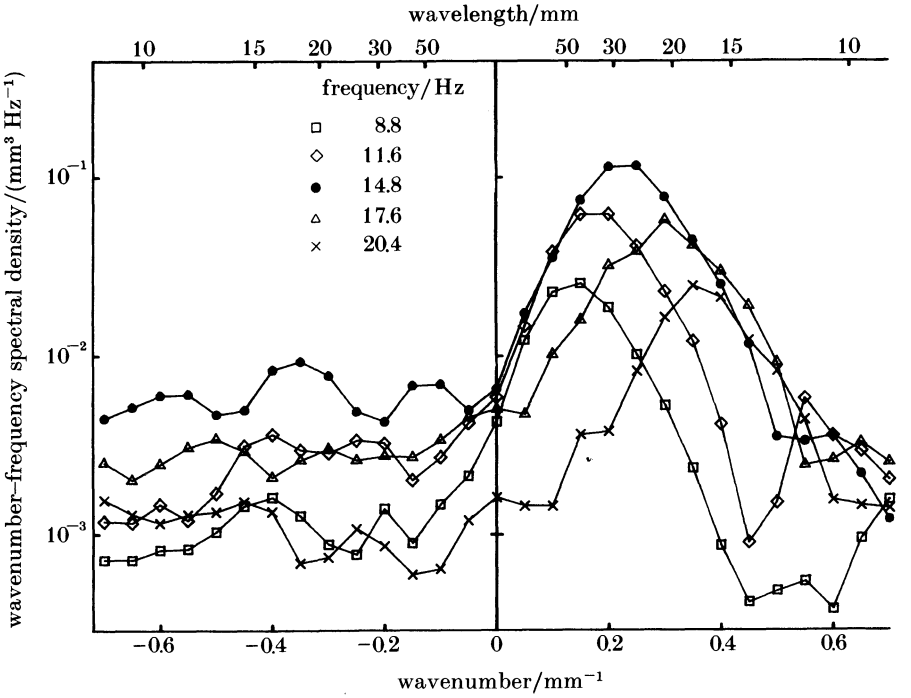

FIGURE 5. Wavenumber distribution of the wavenumber–frequency spectral density, typical of the 0.20 m breaking wave crest region.

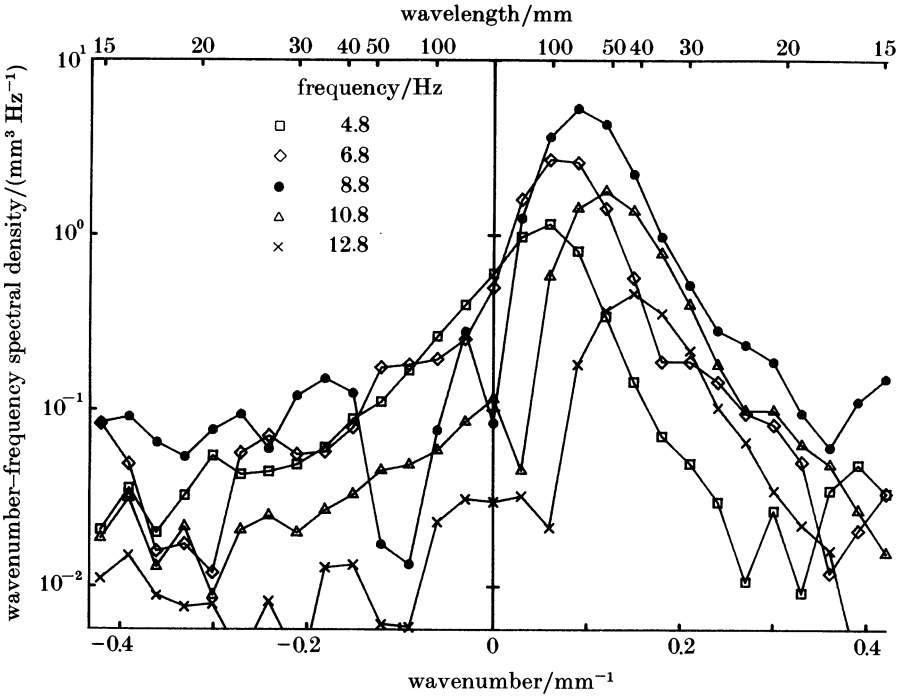

FIGURE 6. Wavenumber distribution of the wavenumber–frequency spectral density, typical of the 0.33 m breaking wave crest region.

spectrum. The phase information associates positive wavenumbers with disturbance modes travelling against the apparent direction of propagation of the breaking wave. It is evident that for both breaking wavelengths, these rearward travelling modes constitute the dominant disturbance modes. From the auxiliary wavelength scale note that the energetic disturbances for both breaking wavelengths occur over a range of order 20–200 mm, with a shift to lower dominant wavelengths with increasing breaking wavelength. While the wavenumber spectra presented here apply in the vicinity of the breaking crest, further rearward the wavenumber spectra are likely to be modified. This aspect has not been pursued here.

The longitudinal and lateral coherence properties of the hydrodynamic disturbances were investigated to provide a broader description of the flow. Figure 7 shows the longitudinal coherence of oscillations at the peak and half power frequencies that arise in the breaking zone and propagate rearward over the 0.33 m breaking wave profile. The fixed probe was held midway between the toe and the crest of the breaking wave. The lateral coherence is shown in figure 8 for the same wave at three sites along the breaking wave profile: in the active breaking region about midway between the toe and the crest, at the crest and about mid-way down the rearward face of the breaking wave. The coherence data for the 0.20 m breaking wave were found to vary in a similar manner. It is apparent that, whereas the longitudinal coherence was persistent over a significant fraction of the breaking wavelength, the lateral coherence scale was much narrower, although tending to

broaden slowly with rearward distance along the breaking wave profile. This data was useful in constructing a physical picture of the structure of the disturbances, as described in §4.

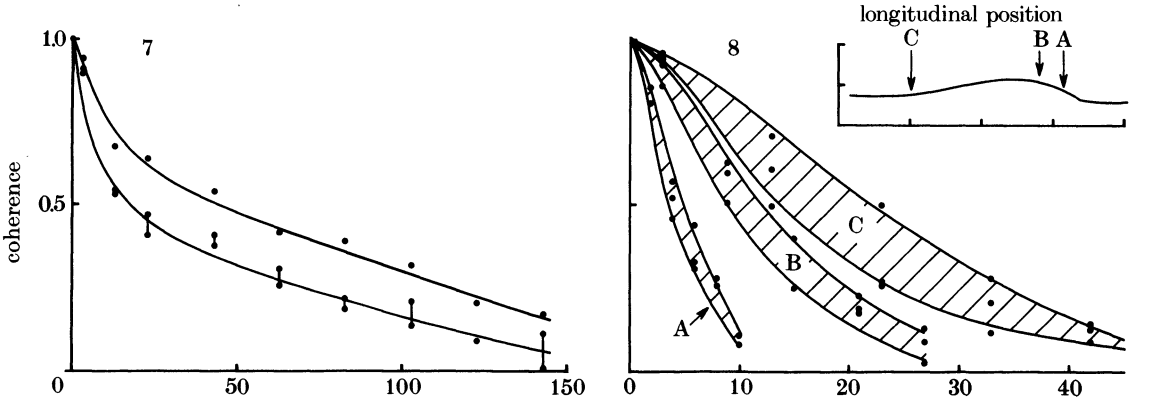

FIGURE 7. Longitudinal coherence of the surface distribution frequency components at the spectral peak (upper trace) and the half-power frequencies (lower trace) for a 0.33 m breaking wave.

FIGURE 8. Lateral coherence of the surface distribution frequency components at the spectral peak and half-power frequencies for three sites along a 0.33 m breaking wave. The inset shows the wave profile from figure 4.

3.2. *X-band microwave reflectivity results*

The microwave backscattered power spectrum was measured with the line of sight centred just ahead of the breaking wave crest as a function of the depression angle for both vertical (vv) and horizontal (hh) transmit–receive polarizations. For brevity, only the vv spectra as shown for, without exception, each corresponding hh spectrum followed extremely closely the vv spectrum for that depression angle, except that the hh spectrum was always reduced by up to 3 dB.

The microwave reflectivity spectra are shown for 'upwind-look' configurations, as shown in figures 9 and 10, for the 0.20 and 0.33 m breaking waves respectively. In figure 9, typical results of reflectivity spectra from unbroken maximally steep waves are indicated, clearly associating the spectral peak with the breaking process. Also shown superimposed is the reference wave gauge disturbance spectrum measured just ahead of the breaking wave crest. The close spectral similarity between the microwave and disturbance spectra is apparent. The interpretation of this fundamental finding is discussed in depth in §4.

To complement the above measurements, which were taken at a fixed axial position centred just ahead of the breaking wave crest, the spatial distribution of the local backscattered microwave power was obtained for a 0.20 m breaking wave at a fixed depression angle of 50°, looking upwind for vv polarization through a 0.10×0.10 m horizontal aperture and is shown in figure 11. For comparison, the spatial distribution over an axially displaced steep unbroken 0.20 m wave is superimposed. There is clearly a sharp mean power peak associated with the

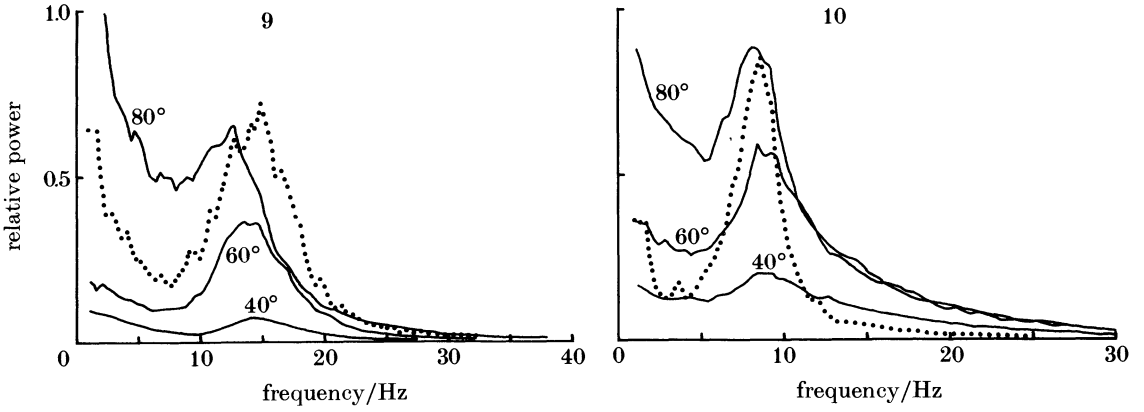

FIGURE 9. Microwave backscattered power frequency spectrum for upwind-look depression angles (solid lines) compared with the surface disturbance frequency spectrum near the 0.20 m breaking wave crest (dotted line).

FIGURE 10. Microwave backscattered power frequency spectrum for upwind-look depression angles (solid lines) compared with the surface disturbance frequency spectrum near the 0.33 m breaking wave crest (dotted line).

breaking zone, located just ahead of the crest in this configuration. The frequency signature of this power peak is contained in the data of figure 3. The mean power per breaking wavelength $\langle P(x) \rangle$ was found by integrating under the breaking wave reflectivity curve and dividing by the breaking wavelength. For the case shown in the figure, $\langle P \rangle \approx 0.047$ units (in terms of the output voltage measured from the crystal detector).

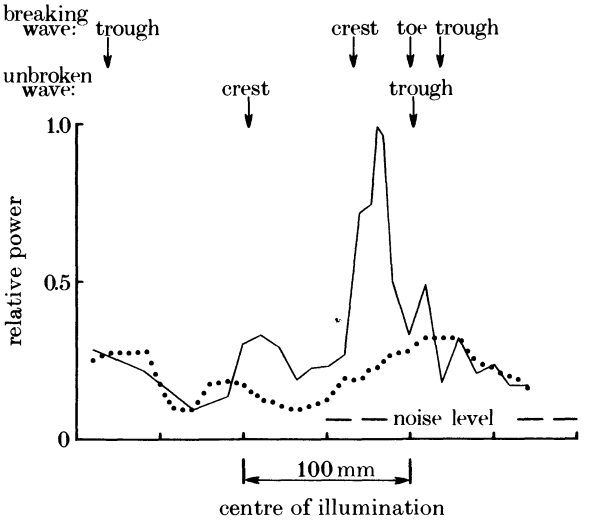

FIGURE 11. Spatial distributions of microwave backscattered power for an upwind-look depression angle of 50° through a 0.10 m aperture length along a 0.20 m breaking wave (solid line) and steep non-breaking 0.20 m wave (dotted line).

For propagating wind waves, monitored as described in §2, typical time series of backscattered power and simultaneous surface elevation are shown for the 3 Hz (mechanically triggered) wind waves in figure 12. It is noteworthy that the microwave signal is characterized by strong local returns from the breaking wave crests. The shape of the signal *in time* is not unlike the *spatial* distribution over the stationary breaking wave shown in figure 11. The temporal mean, $\overline{P(t)}$, was measured to be 0.051 units for this case, in good agreement with $\langle P(x) \rangle$ measured for the stationary wave. Though not reported in detail here, the same close correspondence was found with the microwave beam focused by using a dielectric lens with a 3 dB beam width of 0.15 m, which replaced the need for the aperture. The frequency spectrum of $\overline{P(t)}$, shown in figure 13, shows a secondary peak at around 23 Hz in addition to the main peaks at 3 Hz and its harmonics, which are associated with the passage of breaking wave crests. Allowing for the possible influence of wall effects, the sidewall-mounted optical wave height detector showed evidence of frequency components in the vicinity of 23 Hz, as can be seen in figure 12.

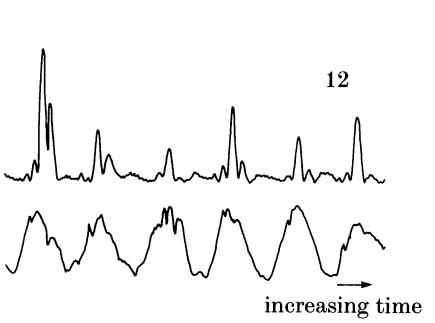

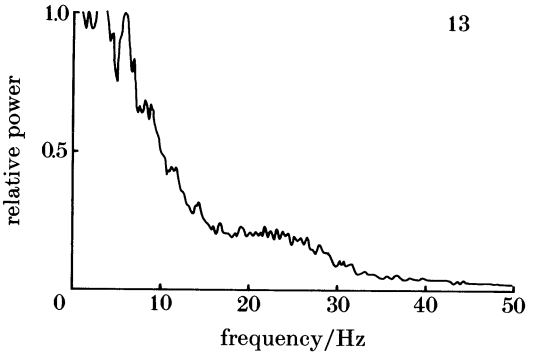

FIGURE 12. A typical 2 s time series of microwave reflected power at an upwind-look depression angle of 50° (upper trace) and simultaneous wave height (lower trace).

FIGURE 13. Frequency spectrum of the backscattered microwave power from time series similar to figure 12.

4. Discussion and conclusions

The association of strong microwave reflectivity with breaking zones of small-scale breaking waves under certain conditions has been noted and considered by previous authors, as described in §1. Here, the results of the present investigation are highlighted and reviewed in the context of explaining this phenomenon.

The spectral investigation of disturbances generated in the spilling zones of small-scale, stationary breaking gravity waves shows that these zones can be regarded as comprising an ensemble of laterally compact, incoherent sources, which radiate longitudinal oscillations that remain coherent in frequency over at least half the breaking wavelength. The corresponding wavelengths of the energetic longitudinal oscillations in the neighbourhood of the breaking wave crest have been investigated. For the 0.20 m breaking wave, the local energetic wavelengths spanned the range 20–50 mm, while for the 0.33 m breaking wave the range was

40 mm to 120 mm. It is believed that these oscillations are instabilities of the strong shear layer formed by the spilling water of the breaking zone flowing over the underlying wave motion.

Setting aside their intrinsic interest as contributors to the high wavenumber–frequency régime of the wave spectrum, breaking zones of short stationary surface waves have been confirmed to be local sources of microwave reflectivity at 9.23 GHz over a wide range of incidence angles in the upwind–downwind direction. Moreover, the frequency of the microwave power return corresponds closely to the hydrodynamic disturbance frequency spectrum. An examination of the frequency–wavenumber spectra reveals that the disturbance wavelengths span the range that satisfies the Bragg resonance condition for the range of depression angles considered here. Corresponding to the upwind-look depression angles of 40°, 60° and 80°, the Bragg condition given by (1) for a 32 mm microwave wavelength yields disturbance wavelengths of 21, 32 and 90 mm respectively. The wavenumber spectra in figures 5 and 6 provide a consistent explanation of the basic mechanism, i.e. Bragg scattering, and of the weak trend to the lower disturbance peak frequencies with increasing depression angle evident in figures 9 and 10. It is apparent that, as the depression angle increases, the energy in the longer Bragg water wavelengths tends to reside in the lower frequency bands. It may be concluded that the data is generally consistent with the Bragg scattering mechanism, as described in §1. However, to establish direct proportionality between the backscattered power and the spectral density of the Bragg water wavenumber as lowest-order Bragg scattering theory predicts is not straightforward because of unknown factors such as (i) uncertainties in the overall microwave power level from a given breaking zone due to the unknown antenna–aperture effects, noise floor levels, etc.; (ii) lack of knowledge of the overall spectral density of the Bragg water-wave wavenumber component, considered over the whole of the illuminated area. Even then, other factors such as Doppler information, which are beyond the scope of the present investigation, would need to be examined.

Microwave backscattering properties determined by using the stationary breaking wave configuration have been compared with corresponding results for propagating breaking wind-waves with similar wavelengths. Their close correspondence supports the use of stationary wave findings in understanding the propagating-wave case. It may be argued that, as a short (centimetric wavelength) gravity wave evolves through a breaking cycle, at each instant the breaking zone produces a peaked disturbance frequency spectrum with an associated wavenumber spectrum distributed over the breaking wave profile rearward from the toe region. The peak frequency may vary from the start to the finish of the breaking cycle but, from the microwave viewpoint, the hydrodynamic disturbance may be regarded as quasi-static. At each stage in this evolution, there will be a subset of disturbance frequencies and wavenumbers that act as described above to produce a strong local microwave power return. To the lowest order, the power contributions of distributed laterally incoherent sources should be additive.

The use of the stationary breaking wave configuration to understand the propagating situation is further strengthened by the following observations. The spectrum of $P(t)$, shown in figure 13, is dominated by the 3 Hz periodicity of

breaking crests moving past the measurement site, resulting in the strong peaks at 3 Hz and its harmonics. This spectrum shows a secondary high frequency signature that peaks at about 23 Hz and appears attributable to the rapid, oscillatory structure within the bursts of microwave backscattered power evident in the time series of figure 12. This is believed to be the counterpart of the strong peaked response observed in the stationary breaking wave microwave power measurements. Owing to resolution limitations of the wave-height probes, a 23 Hz oscillation signature was not readily detected in the height signal of the propagating breaking waves. However, when using the optical sidewall meniscus probing technique, the time series did reveal the presence of oscillations of this frequency around the crests. An example is shown in figure 12. Finally, it is of interest to reconcile the 14.4 Hz peak for the stationary breaking wave at a depression angle of 50° with the 23 Hz peak observed for the propagating case. The dominant Bragg wavelength near the stationary 0.20 m breaking wave crest for a 50° depression angle was determined to be approximately 0.025 m, with a backward phase speed of $0.025 \times 14.4 = 0.36$ m s^{-1} relative to the stationary wave crest. The centreline windspeed, $U_c = 7.5$ m s^{-1}, forcing the mechanically triggered 3 Hz waves is known to induce an average wind drift current V_s of about $0.03U_c \approx 0.23$ m s^{-1}. Figure 4 of Wu (1975) summarizes the influence of the surface wind drift on the phase speed of water waves in the frequency range 1–200 rad s^{-1}. In this figure, C_m is the measured phase speed, C_0 is the infinitesimal slope phase speed and V_s is the surface wind drift velocity. The data show the variation of $(C_m - C_0)/V_s$ as a function of wave frequency σ (for 3 Hz waves $(C_m - C_0)/V_s \approx 0.4$ with $C_0 = 0.525$ m s^{-1}, $V_s = 0.23$ m s^{-1} and $C_m \approx 0.62$ m s^{-1}). For higher-frequency waves corresponding to a wavelength of 0.025 m, $\sigma \approx 70$ rad s^{-1}, for which $(C_m - C_0)/V_s \approx 0.6$. This indicates that the 0.025 m disturbance phase speed is likely to be modified by about $0.6\ V_s \approx 0.15$ m s^{-1}. Hence the apparent phase speed to a stationary observer of the 0.025 m disturbances will be approximately

$$-0.36 + 0.62 + 0.15 = 0.41 \text{ m s}^{-1},$$

resulting in an apparent frequency of $0.41/0.025 \approx 16.5$ Hz. Even allowing for the uncertainties in these estimates, this apparent frequency is lower than the observed secondary peak at 23 Hz. These estimates have been based on average wind-drift effects for 'free' water-wave components. However, there appears to be justification from the findings of Okuda *et al.* (1977) that the use of an average wind drift correction could underestimate significantly the local effect on the propagation of the short disturbance components generated in breaking zones. Okuda *et al.* (1977) reported strong enhancement of the wind drift shear levels for the water surface layer that feeds into the breaking zones of short wind-waves. By implication, the surface layer speed would be enhanced near the breaking crests, which in turn would act to reduce the rearward propagation speed. It is known from the findings of Keulegan (1951) that the average wind drift of $0.03U_c$ is obtained either for surfaces covered with slicks that suppress almost all the wind-wave motions or the other extreme, in the presence of almost continually breaking wind-waves. The separated airflow associated with breaking waves implies, locally, that the wind drift is negligible over a significant fraction of the (breaking) wave: this fraction

was determined to be about one-half according to Okuda *et al.* (1977). Hence a local doubling of the effective wind drift on the windward face of the breaking zone would not be inconsistent with their findings. This would increase the apparent frequency as estimated above by $0.15/0.025 \approx 6$ Hz and would reconcile the stationary and propagating wave spectral signatures.

The experimental evidence presented here provides an explanation for the observations of Wright *et al.* (1972) on the question of dominant Bragg scatterers observed to be nearly bound to the wind-driven dominant waves rather than propagating as 'free' waves. The breaking zone disturbances investigated here tend to have phase speeds close to the dominant wave, i.e. the backward speed of a typical short resonant wavenumber component, relative to the breaking zone generating it, being offset to a large extent by forward wind drift effects and resulting in the approximate forward phase speed close to that of the dominant wave. In addition, the local frequency relative to the breaking wave of the resonant wavenumber component decreases with increasing breaking wavelength, according to our data. Thus its rearward speed decreases as the dominant breaking wavelength increases, tending to enhance the bound Bragg scatterer effect at larger fetches or durations for a given windspeed. These findings also provide a 'physical' basis for the observations of Kwoh & Lake (1983) in terms of the Bragg scattering mechanism without recourse to 'specular' scattering. Given the physical scales of the breaking zone structure and the microwave return spectra reported here, it is difficult to envisage that conditions appropriate to specular backscatter (i.e. locally planar surfaces over many microwave wavelengths) exist in these regions.

For ocean wave microwave modulation experiments at 9.375 and 1.5 GHz, Wright *et al.* (1980) report modulation levels for microwave power backscattered from long ocean waves measured from an ocean platform. These modulation levels were found to be unaccountably high, based on the estimated contributions of tilting, range variation and hydrodynamic modulation to the variability of the Bragg water wavenumber component of the short-wave spectrum. A recent optical determination of short-wave modulation with long ocean gravity waves by Monaldo *et al.* (1982) yielded modulation transfer functions for typical Bragg wavelengths which do not account convincingly for the observed microwave modulation data, as described in §1. The present study has demonstrated strong localized microwave backscatter from small-scale breaking waves. Casual observation suggests that small-scale breaking events are modulated by the long waves and tend to occur near the long-wave crests, often predominantly on the leeward side. Modulation of these compact sources of backscatter is a potential contributor to the microwave backscatter modulation transfer function.

The present contribution also elucidates a spikey feature of radar backscatter, known as 'sea spikes', often observed for high sea states. This has been reported by Alpers *et al.* (1981), who summarize the findings of other investigators, pointing out the strong correlation of the occurrence of sea spikes with breaking waves. They conclude with the expectation that 'sea spikes are an important phenomenon in wave imaging for high sea states'.

An important question that emerges from this study is the relative contributions to the backscattered cross section for oceanic conditions of 'free' Bragg waves and

the Bragg waves emanating from the breaking zones of small-scale breaking waves. From the N.R.L. study of Wright *et al.* (1972) it would appear that the relative importance depends on the look angle, windspeed and fetch. Wave tank conditions can depart considerably from field conditions, so that their study is not necessarily representative of the oceanic case. The orbital advection by the long ocean wave spectrum makes it difficult to separate the two effects via local Doppler measurements of microwave backscatter. Concomitantly, there is the added unknown complication that long-wave modulation of the local windstress might introduce in attempting to predict the underlying shortwave dynamics. Thus this problem remains a challenging one. Further work along these lines should improve our understanding of microwave modulation by wind-driven ocean waves and would be of considerable value in choosing optimal viewing geometries of future satellite-based active microwave sensors and in interpreting more accurately the oceanographic information from these remote-sensing techniques.

Much of this work was done while the first author was a visiting Senior Research Scientist at the Royal Australian Navy Research Laboratory. The support of this laboratory, the Water Research Laboratory at the University of New South Wales and the Australian Research Grants Scheme is gratefully acknowledged. Discussions with Dr I. S. F. Jones were very useful in the course of the investigation.

References

Alpers, W. R., Ross, D. B. & Rufenach, C. L. 1981 *J. geophys. Res.* **86**, C9, 6481–6498.
Duncan, J. R., Keller, W. C. & Wright, J. W. 1974 *Radio Sci.* **9**, 809–819.
Keller, W. C. & Wright, J. W. 1975 *Radio Sci.* **10**, 139–147.
Keulegan, G. H. 1951 *J. Res. natn. Bur. Stand.* **46**, 358–381.
Kwoh, D. S. W. & Lake, B. M. 1983 *T.R.W. Rep.* no. 37564-6001-UT-00. T.R.W. Space and Technology Group, California 90278.
Lee, P. H. Y. 1977 *J. Fluid Mech.* **81**, 225–240.
Monaldo, F. M. & Kasevich, R. S. 1982 *IEEE Trans. Geosci. remote Sensing* **GE-20**, 254–258.
Okuda, K., Kawai, S. & Toba, Y. 1977 *J. oceanogr. Soc. Japan* **33**, 190–198.
Plant, W. J. & Wright, J. W. 1977 *J. Fluid Mech.* **82**, 767–793.
Wright, J. W., Duncan, J. R. & Keller, W. C. 1972 *N.R.L. Rep.* no. 7473. Naval Research Laboratory, Washington D.C.
Wright, J. W., Plant, W. J., Keller, W. C. & Jones, W. L. 1980 *J. geophys. Res.* **85**, C9, 4957–4966.
Wu, J. 1975 *J. Fluid Mech.* **68**, 49–70.

ERRATA

Proc. R. Soc. Lond. A **399**, 93–109 (1985)

On the microwave reflectivity of small-scale breaking water waves

BY M. L. BANNER AND E. H. FOOKS

Page 100, figure 3, *for* 0.02 *read* 0.16.
Page 100, figure 4, *for* 0.3 *read* 1.75.
Page 101, figure 5, each vertical graduation should be multiplied by 8.
Page 102, figure 6, each vertical graduation should be multiplied by 5.83.